JOURNAL OF MAPS
2025, VOL. 21, NO. 1, 2472779
https://doi.org/10.1080/17445647.2025.2472779

SCIENCE

OPEN ACCESS Check for updates

Miocene stratigraphy and vertebrate paleontology along the western side of Cerros Cadena de los Zanjones (East Pisco Basin, Peru)

Giulia Bosio [a], Alberto Collareta [a], Matteo Pedini [b], Maria Elena Gastaldello [c], Francesco Nobile [a], Luca Pellegrino [d], Pietro Paolo Pierantoni [b], Elisa Malinverno [c], Olivier Lambert [e], Giuseppe Marramà [d], Walter Landini [a], Giorgio Carnevale [d], Rafael Varas-Malca [f,g], Claudio Di Celma [b], Stefano Mazzoli [b], Mario Urbina [f] and Giovanni Bianucci [a]

[a]Dipartimento di Scienze della Terra, Università di Pisa, Pisa, Italy; [b]Scuola di Scienze e Tecnologie, Università di Camerino, Camerino, Italy; [c]Dipartimento di Scienze dell'Ambiente e della Terra, Università di Milano-Bicocca, Milano, Italy; [d]Dipartimento di Scienze della Terra, Università di Torino, Torino, Italy; [e]D.O. Terre et Histoire de la Vie, Institut Royal des Sciences Naturelles de Belgique, Brussels, Belgium; [f]Departamento de Paleontología de Vertebrados, Museo de Historia Natural-UNMSM, Lima, Peru; [g]Unidad de Paleontología, Museo de Historia Natural, Universidad Ricardo Palma, Lima, Peru

ABSTRACT

The Miocene Pisco Formation (East Pisco Basin, Peru) is renowned for its abundant, well-preserved fossils of marine vertebrates, representing one of the most spectacular and complete records of Neogene marine vertebrates worldwide. Here, we present a geological map at 1:10,000 scale investigating the spatial and temporal distribution of fossil vertebrates at Cerros Cadena de los Zanjones, in the Ica River Valley. Stratigraphic and paleontological analyses reveal the widespread occurrence of marine vertebrate remains in the Tortonian (10.0–8.6 Ma) P1 and Tortonian – Messinian (8.4–6.9 Ma) P2 sequences. These include 91 specimens preserved as bony elements, including cetaceans (both Odontoceti and Mysticeti), seals (Pinnipedia) and bony fishes (Osteichthyes). Elasmobranchs, including Carcharhiniformes, Lamniformes and Myliobatiformes, are represented by some 300 teeth. The P1-P2 passage is marked by faunal novelties such as the first appearance of seals. Overall, the assemblage taxonomically resembles that of the nearby, well-investigated site of Cerro Colorado.

ARTICLE HISTORY
Received 20 December 2024
Revised 18 February 2025
Accepted 20 February 2025

KEYWORDS
Facies analysis; structural analysis; paleontological heritage; Pisco formation; Tortonian; Messinian

1. Introduction

The Pisco Formation of southern coastal Peru is a well known stratigraphic unit that owes its celebrity to its extraordinary fossil content, offering profound insights into the Miocene evolution of marine ecosystems (e.g. Bianucci & Collareta, 2022; Bosio et al., 2021; Lambert et al., 2010). Indeed, the Pisco Formation cropping out in the Ica River Valley is home to an abundant and scientifically significant fossil fauna that includes marine vertebrates such as whales, dolphins, porpoises, seals, seabirds, marine turtles, crocodiles, and bony and cartilaginous fishes, all reflecting thriving ancient ecosystems (e.g. Bianucci et al., 2016a, 2016b, 2024; Collareta et al., 2021b; Lambert et al., 2010; Stucchi et al., 2015). This wealth of fossils makes the Pisco Formation invaluable for different studies in a variety of topics concerning the evolutionary paleoecology of the marine biosphere, thereby offering useful insights for the reconstruction of the evolutionary and ecological dynamics of the Neogene marine faunas of the southeastern Pacific Ocean (Collareta et al., 2021b). Detailed sedimentological, taphonomic and geochemical studies have also revealed complex depositional and early diagenetic histories, which played a critical role in the often-exceptional preservation of fossils (Bosio et al., 2021; Gariboldi et al., 2015; Gioncada et al., 2016, 2018). Such discoveries further underscore the importance of the Pisco Formation as a paleontological hotspot and a natural archive of ancient marine life, highlighting the importance of preserving this unique paleontological heritage.

Here, we present a 1:10,000-scale geological map (Main Map) covering an area of approximately 37 km² along the western side of Cerros Cadena de los Zanjones, a new fossil-bearing locality of the Pisco Formation. This work builds upon earlier geological surveys (Di Celma et al., 2016a, b, 2022), and integrates new biostratigraphic and structural data, providing the groundwork for more detailed paleontological investigations and interpretations. The marine fossil vertebrates identified within these strata are systematically documented on the geological map and along two measured sections,

CONTACT Claudio Di Celma claudio.dicelma@unicam.it Scuola di Scienze e Tecnologie, Polo di Geologia, via Gentile III da Varano, 7, Camerino, MC 62032, Italy

Supplemental map for this article is available online at https://doi.org/10.1080/17445647.2025.2472779.

illustrating their horizontal and vertical distribution in this area.

2. Geological and stratigraphic setting

The study area is located along the South American convergent margin, which is primarily characterized by erosional rather than accretional processes (Clift & Vannucchi, 2004; Noda, 2016). The forearc basin system of the Peruvian region is notably segmented across the margin and further divided by the Outer Shelf High, a northwest-trending structural high consisting of the Precambrian-Paleozoic basement. This configuration leads to the development of an inner and an outer set of elongated basins running parallel to the trench (Kulm et al., 1982; Thornburg & Kulm, 1981). The subsidence and uplift history within these forearc basins reflect the complex interaction between the subducting Nazca Plate and the overriding South American Plate along the Peruvian convergent margin (Herbozo et al., 2020; Viveen & Schlunegger, 2018; von Huene & Suess, 1988).

The forearc region of Peru is located landward of where the aseismic Nazca Ridge collides with the continental margin (Ciattoni et al., 2025 and references therein) and consists of the onshore East Pisco Basin (EPB) and the offshore West Pisco Basin (WPB) (Figure 1a). These basins are separated from each other by the Coastal Cordillera structural high, which represents the landward extension of the Outer Shelf High (Romero et al., 2013).

The sedimentary fill of the EPB is organized into two megasequences, namely, megasequences P (Paleogene) and N (Neogene), both of which are bounded by significant unconformities that mark critical phases of the basin evolution (Di Celma et al., 2022). Megasequence N, which includes the Miocene Chilcatay and Pisco formations, lies above megasequence P and locally onlaps the eroded crystalline basement. Stratigraphic analyses of the Chilcatay and Pisco formations have identified several key internal stratigraphic surfaces, which permitted the recognition of high-frequency sequences within each formation (Di Celma et al., 2017) (Figure 1b). In particular, based on the presence of three widespread erosional surfaces, called PE0.0, PE0.1 and PE0.2 from oldest to youngest, the Pisco Formation can be subdivided into three main sequences designated as P0 (14.7–12.6 Ma), P1 (10.0–8.6 Ma) and P2 (8.4 to ≥ 6.71 Ma) (Bosio et al., 2020a, 2020b, 2022; Gariboldi et al., 2017; Malinverno et al., 2025). Based on sedimentological analysis, the Ct1 sequence mainly comprises conglomerates and bioclastic sandstones divided into three facies associations recording deposition in shoreface, offshore, and subaqueous delta settings. The Ct2 sequence comprises two facies associations, recording deposition in shoreface (sandstones) and offshore (siltstones) settings (Di Celma et al., 2019). The overlying Pisco Formation is characterized by three transgression cycles (P0, P1 and P2), each comprising a shoreface (fine-grained sandstones and coarse siltstones) and an offshore (diatomaceous mudstones) setting (Di Celma et al., 2017).

3. Surveying methods

The study area is located along the western side of Cerros Cadena de los Zanjones (Figure 1c). Although the stratigraphy of the Pisco Formation is relatively straightforward at this site, the occurrence of a complex network of faults complicates the efforts to provide a detailed correlation of the faunas in laterally separated areas (Figure 2). Consequently, the study area required comprehensive geological and structural mapping to unravel its intricate and dispersed features. Fieldwork focused on documenting the faults, including analyses of their geometry, kinematics and dimensional attributes, as well as on quantifying fault displacements wherever feasible. These efforts were complemented by the interpretation of recently available high-resolution imagery (a few meters per pixel or less) from Google Earth, which provided valuable insights into the spatial arrangement and characteristics of the fault system (see Tewksbury et al., 2012 for methods for mapping bedrock structures in remote areas in Google Earth). The stratigraphy of the exposed succession was established through detailed sedimentological logging of two reference stratigraphic sections (Figure 2a, b), geological mapping at 1:10,000 scale and facies analysis. Two sedimentary sections, namely, CCZ (western side of Cerros Cadena de los Zanjones; base: 14°34′12.6″S, 75°43′44.8″W; top: 14°34′39.3″S, 75°43′10.2″W) and CLQw (further north, western side of Cerro los Quesos; base: 14°31′2.2″S, 75°43′11.1″W; top: 14°31′13.2″S, 75°44′33.7″W), measuring respectively 175 and 130 m (Figure 2), were measured using a high-precision Jacob's staff with rotatable laser pointer (see Patacci, 2016). Log descriptions included information such as bed thickness, lithology, estimation of grain size (using a comparator and a hand lens), type of sedimentary structures and bioturbation intensity. Age constraints for the exposed sedimentary succession allow for basin-wide correlations across vast tracts of inaccessible desert, and are provided by $^{40}Ar/^{39}Ar$ radiometric dating of volcanic ash layers (Bosio et al., 2020b) and biostratigraphic analyses using diatoms based on 45 rock samples. These samples were collected along the two measured sections with a spacing of about 1–2 m and integrated with 14 additional samples collected at a previously unmapped site at the south-western end of the study area. As for the paleontological prospecting, each vertebrate specimen encountered in situ during the survey had its

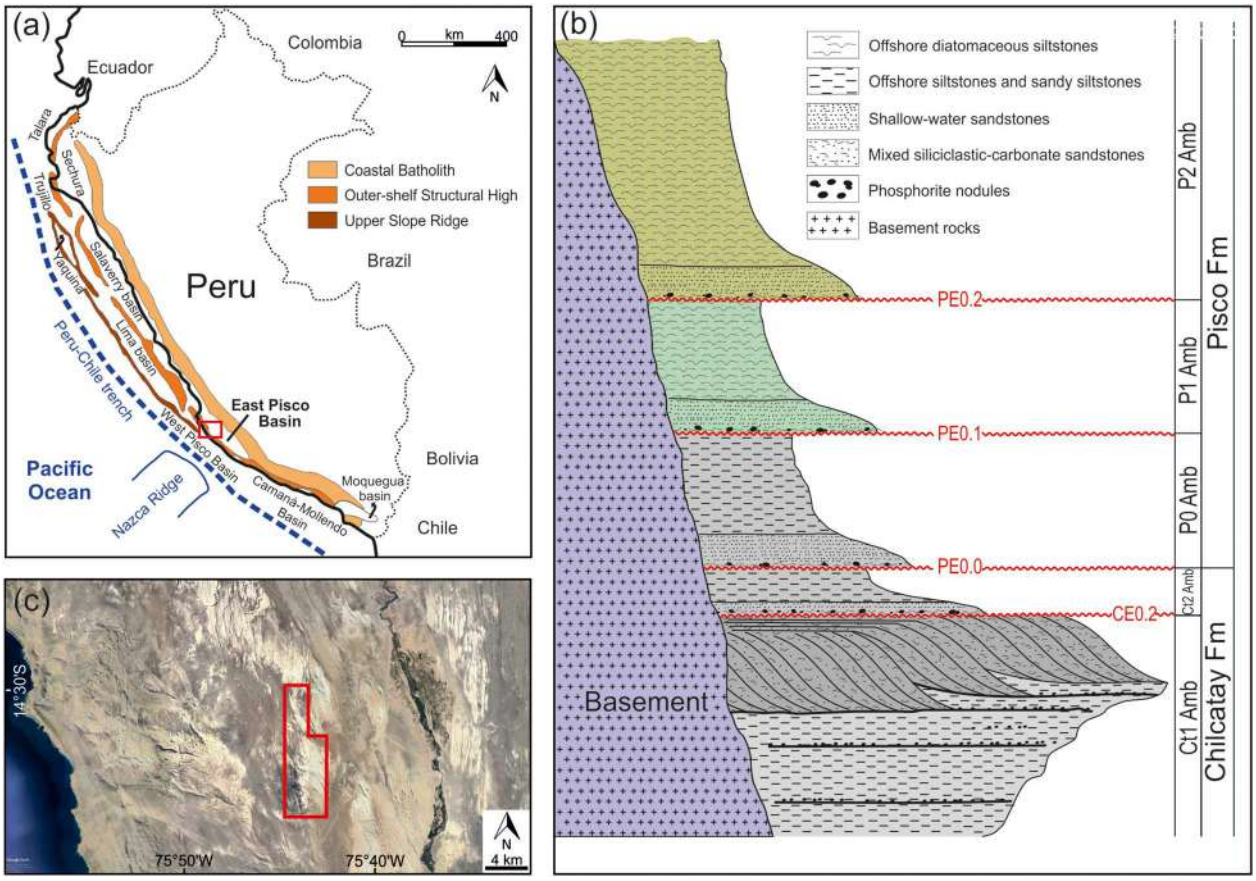

Figure 1. Geological and stratigraphic framework. **(a)** Map of the major Cenozoic sedimentary basins along the Peruvian coast, with indication of the major structural highs, i.e. the Coastal Batholith, the Outer Shelf High and the Upper Slope Ridge. Redrawn and modified after Travis et al. (1976) and Thornburg and Kulm (1981). The red box indicates the study area in the East Pisco Basin. **(b)** Schematic stratigraphic column of the Chilcatay and Pisco formations, and their internal subdivision into high-frequency sequences. Modified after Di Celma et al. (2018a). The green-colored sequences are those cropping out at this locality. The vertical scale is only indicative of thickness of sediment packages between unconformity surfaces. **(c)** Satellite image showing the geographic location of the study area along the western side of the Ica River valley (outlined by a red frame).

geographic location recorded with a handheld GPS, while its stratigraphic position along the measured sections was determined with an accuracy of ±0.4 to ±3 meters. The horizontal and vertical distribution of all recorded fossils in the study area is presented in the Main Map, which reports two sections, namely CCZ (for specimens from the southern part of the study area) and CLQw (for those from the northern part thereof). Similar to previous studies in fossil-rich areas of the Ica Desert (Di Celma et al., 2018b, 2019, Bianucci et al., 2016a, b; Collareta et al., 2021a), we prospected the study area by providing taphonomic characterizations and preliminary taxonomic identifications directly in the field. Depending on the nature of the skeletal parts that were preserved or exposed in the field, more or less accurate systematic determinations could be made, based also on comparisons with several well-investigated specimens from other Upper Miocene localities of the Ica Desert (Bianucci & Collareta, 2022; Bianucci et al., 2010, 2016c, 2024; Collareta et al., 2015; de Muizon, 1981, 1988; Dewaele & de Muizon, 2024, Lambert & de Muizon, 2013, 2021; Landini et al., 2017a, b). Only a few noteworthy specimens were collected for storage at the Museo de Historia Natural de la Universidad Nacional Mayor de San Marcos (MUSM) in Lima. As for the elasmobranchs (sharks and rays), only the teeth with precise GPS coordinates were consistently plotted on the map and included in the stratigraphic column. Similar to what was done for the marine tetrapods, the taxonomic identification of the elasmobranch finds was supported by comparisons with well-studied coeval materials from other outcrops of the Pisco Formation (Landini et al., 2017a).

4. Stratigraphic and structural overview

4.1. Stratigraphy and age

In the study area, only the Upper Miocene P1 and P2 sequences of the Pisco Formation are exposed. Sequence bounding unconformities are omission surfaces commonly demarcated by a *Glossifungites* ichnofacies and are interpreted as composite discontinuities that formed during a phase of relative sea-level fall to be subsequently modified during the onset of

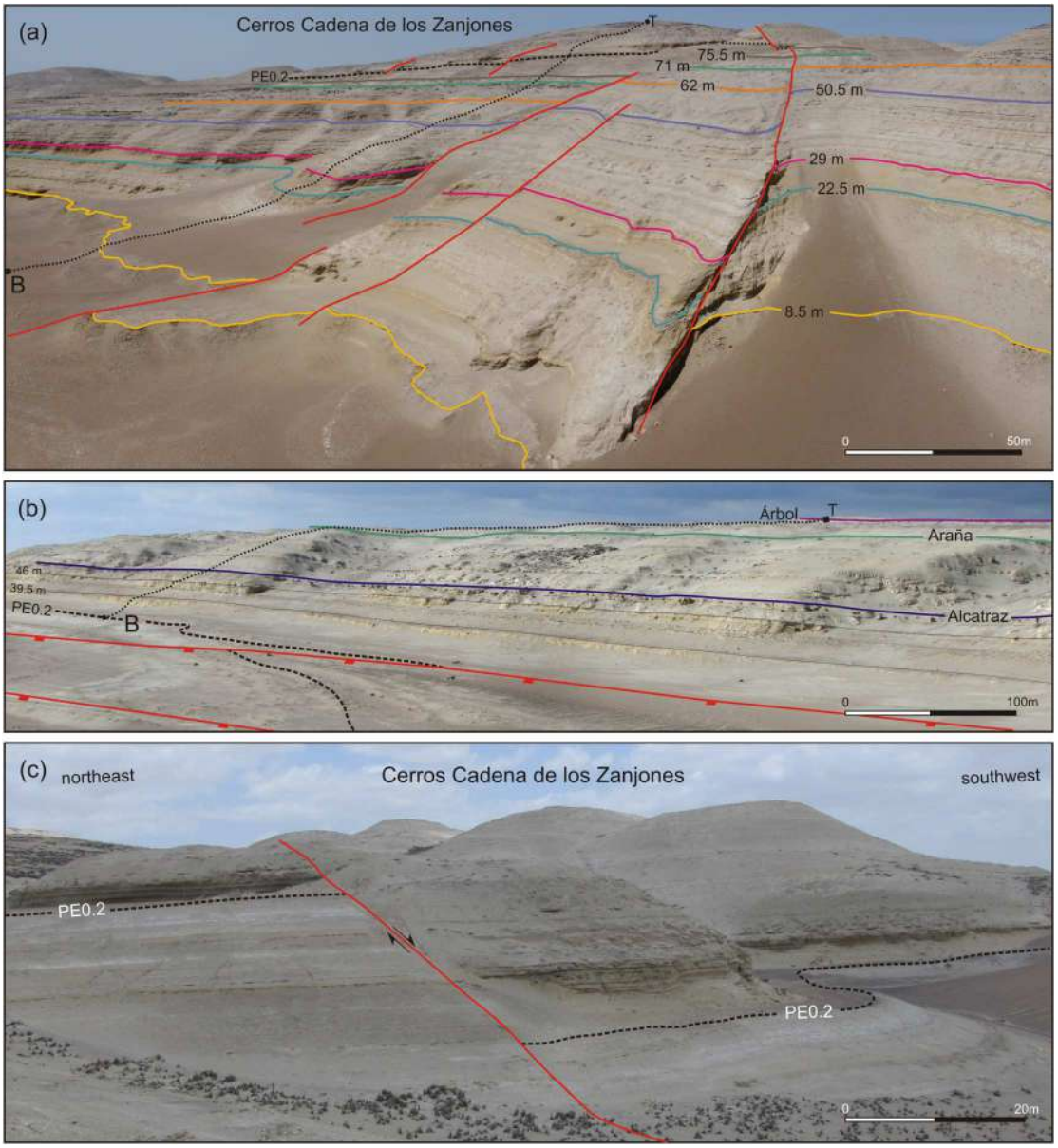

Figure 2. Panoramic views showing the locations of the two measured sections and field examples of small-displacement normal faults (depicted as solid red lines) dissecting the studied succession. Numbers indicate the stratigraphic height (in meters) along the individual measured sections. **(a)** Oblique aerial view of the western side of Cerros Cadena de los Zanjones, showing the position of the CCZ measured section (B, base: 14°34′12.6″S, 75°43′44.8″W; T, top: 14°34′39.3″S, 75°43′10.2″W) and examples of small-displacement normal faults offsetting some of the main marker beds (colored lines). View is toward the southeast. **(b)** View of the western side of Cerro Los Quesos showing the position of the CLQw measured section, at the northern end of the study area (base: 14°31′2.2″S, 75°43′11.1″W; T, top: 14°31′13.2″S, 75°44′33.7″W). Names of main marker beds as in Di Celma et al. (2016a). View is toward the northeast. **(c)** Decameter-scale normal fault surface (colored as red) cutting through the PE0.2 unconformity (black dashed lines) at Cerros Cadena de los Zanjones.

transgression (Di Celma et al., 2017, 2018a). Each sequence is characterized by a coarse-grained basal portion, representing deposition in distal lower shoreface to inner shelf settings, which progressively grades upward into finer-grained, offshore sediments. Usually, the base of each sequence consists of a thin conglomerate layer comprised of well-rounded, pebble-sized phosphate nodules, mollusk shells, sporadic polished vertebrate bones and teeth, and subangular to rounded crystalline cobbles and boulders (Bosio et al., 2024). Overlying this lag, a package of massive orange sandstones and coarse siltstones characterizes the first meters of the measured sections. These sandstones are often moderately to highly bioturbated and exhibit local sedimentary structures such as unidirectional cross-lamination, swaley cross-stratification and wave ripples. These structures indicate deposition in a shoreface setting strongly influenced by storms (Chiocci & Clifton, 1991; Leckie & Walker, 1982; Myrow, 1992). The overlying, fine-grained sediments are made up of finely laminated, gray to white diatomites or diatomaceous siltstones rich in planktic and benthic diatoms, reflecting a low-energy, highly productive,

offshore marine environment (Gariboldi et al., 2023). Associated lithologies include thin layers of fine – to medium-grained sandstone, dolomitized mudstone beds (Malinverno et al., 2023), and andesitic to rhyolitic, metaluminous to peraluminous volcanic ash layers (Bosio et al., 2019). These fine-grained ashes represent the distal, crystal-depleted falls of large explosive eruptions, dispersed from the eruption column or from a co-ignimbrite ash-cloud (Fisher & Schmincke, 1984) following the volcanic activity in the Eastern and Western Cordillera of the Central Andes (Bosio et al., 2020c). They allow for the $^{40}Ar/^{39}Ar$ dating and tephrostratigraphic correlation of sections several kilometers apart, thus greatly increasing the chronostratigraphic detail.

At Cerros Cadena de los Zanjones, the lower portion of the P1 sequence is exposed along the CCZ section. It is dated to the Tortonian thanks to two ash layers, namely, ZANJ-T6 (3 m above the base of the section, hereinafter abs) and LA(16) (8 m abs), which provide radiometric ages of 9.46 ± 0.05 Ma and 9.00 ± 0.02 Ma, respectively (Bosio et al., 2020b). Along the CLQw section, an ash layer at the base of P1 gives an age of 9.31 ± 0.01 Ma (ANF-T1) (Bosio et al., 2020b). This age framework is further supported by diatom biostratigraphy. Specifically, the co-occurrence of the diatom marker species *Lithodesmium reynoldsii* and *Denticulopsis praekatayamae* from 15–66 m abs along the CCZ section constrains this interval between 9.6 Ma (First Occurrence, hereinafter FO, of *D. praekatayamae*) and 9.0 Ma (Last Occurrence, hereinafter LO, of *L. reynoldsii*) (ranges of taxa according to Lazarus et al., 2014). The lowest few meters of the succession, known by samples from the southwestern edge of Cerros Cadena de los Zanjones, include *Denticulopsis vulgaris* but lack both *D. praekatayamae* and *L. reynoldsii*, and as such, are probably slightly older than 10 My, as reported for the basal layers of the P1 sequence at Cerro Tiza (Malinverno et al., 2025). The top of P1 has been dated through the ZANJ-T3 tephra (92 m abs, CCZ section) that yields an age of 8.60 ± 0.11 Ma, whereas the LO of *D. praekatayamae* (8.6 Ma) is locally recognized 83 m abs (Bosio et al., 2020b). The base of the overlying P2 sequence is dated to 8.39 ± 0.03 Ma in the CLQw section thanks to the $^{40}Ar/^{39}Ar$ dating of the ash layer ANF-T4 (Bosio et al., 2020b). In the study area, the age of the P2 strata has been estimated based on the radiometric dating of ZANJ-T28 (161 m abs, CCZ section), which provides an age of 7.62 ± 0.11 Ma, 14 m below the top of the measured section (Bosio et al., 2020b). Furthermore, the occurrence of *Fragilariopsis pliocena* between 122–163 m along the CCZ section constrains this interval between 8.0 and 6.9 Ma (corresponding to the FO and LO of *F. pliocena*, respectively), whereas the FO of *Fragilariopsis reinholdii* (7.7 Ma) is recognized ca. 73 m abs along the CLQw section.

4.2. Structural framework

A detailed field-based structural analysis was conducted to characterize the numerous faults that cut through the stratigraphic succession exposed in the study area (Figure 3a). These faults display variable normal offsets, ranging from decimeter – to several meter-scale, with maximum displacements up to ~50 m in the northern part of the study area. Two main orientations are observed, namely, a set of NW – SE-striking faults, and a subordinate set of NNE – SSW-striking faults. A comparison of our field data with satellite-derived lineament orientations (Figure 3a) reveals consistent primary trends in both datasets, with dominant strikes in the range of N130–150°. The secondary fault set, striking roughly N30°, was identified by means of field observations and is less prominent in satellite data. That said, the fault sets identified in the study area are generally consistent with those outlined by Viveen and Schlunegger (2018) based on the interpretation of satellite imagery and field-based structural mapping, which led those authors to recognizing three main sets of large-scale faults and lineaments within the EPB, striking approximately N160°, N120° and N30°, respectively (Figure 3c-d).

Fault planes are planar, with dip angles ranging between 65–75°, and fault lengths vary from a few hundred meters to a maximum of 4 km (mean: 500 m; median: 400 m). Through a detailed field survey, 173 fault attitude measurements and associated kinematic indicators, such as slickenlines and slickenfibers, were collected along fault planes (Figure 3b, c). These data indicate that extensional dip-slip faulting dominates both fault sets. Constraining the timing of these structures is challenging, with field evidence suggesting that they postdate the deposition of P2. On the other hand, some of the normal faults appear to control thickness variations within the Pisco Formation, thus suggesting a Miocene, syn-sedimentary extensional activity.

In the central and northern portions of the study area, the Pisco Formation strata generally dip at low angles (5–10°). In the southern portion, the lower strata of the P1 sequence are involved in a gentle anticline-syncline fold pair. These gently south-plunging folds are characterized by interlimb angles of approximately 165°. Within the area outlined by the dotted square in Figure 3a, 191 bedding attitudes were recorded. Structural analysis was undertaken using Stereonet v.11 software (Allmendinger et al., 2012; Cardozo & Allmendinger, 2013), including the elaboration of stereonet plots and best-fit great-circles (π diagrams) of bedding pole distributions (Figure 3e). The results indicate a sub-horizontal fold axis plunging 8° toward N189° (Figure 3a). These folds appear

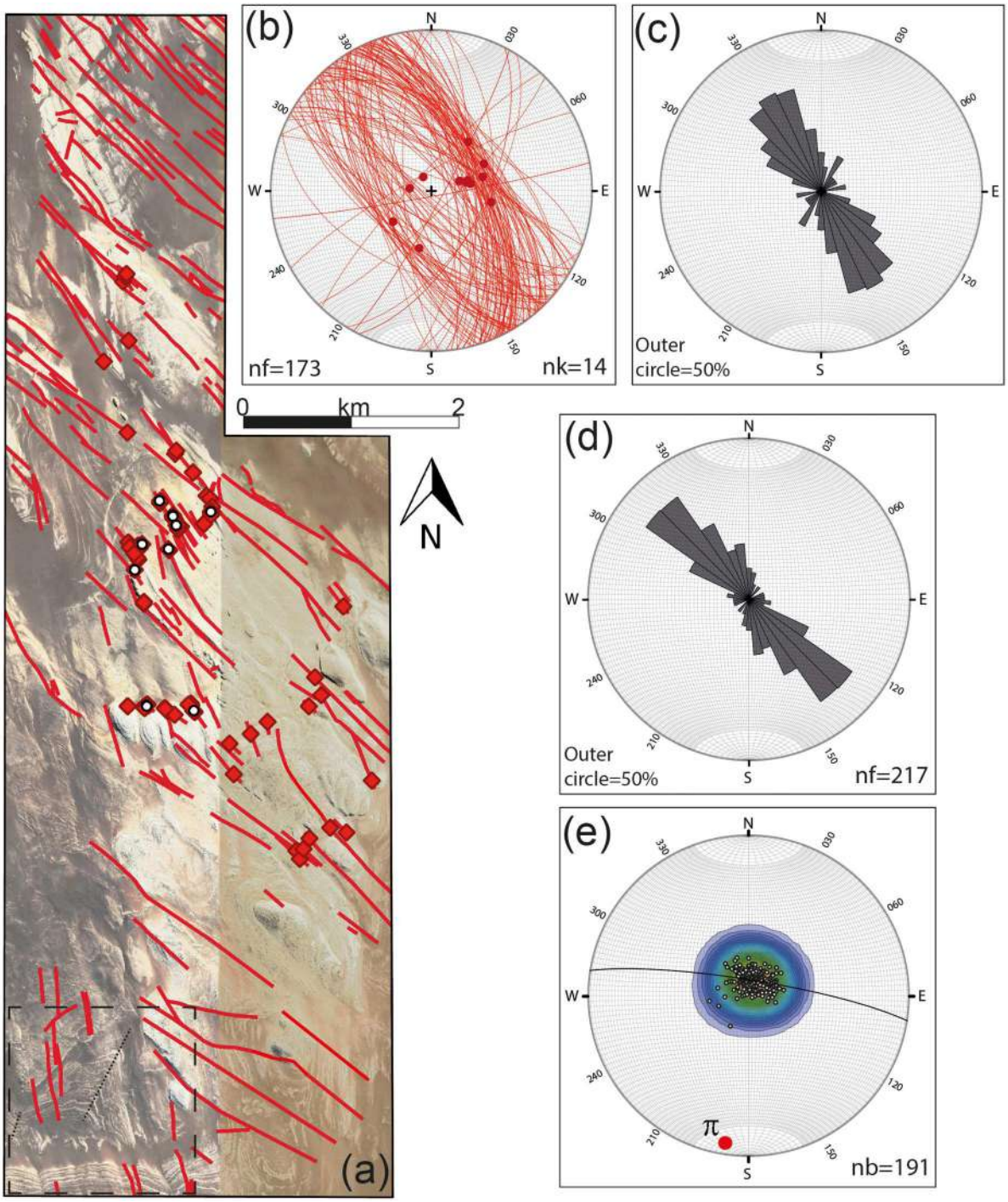

Figure 3. Structural map of the study area. **(a)** Map view from Google Earth, showing the study area (outlined by the black perimeter line; see Figure 1). Red lines represent fault traces identified through satellite image analysis. Red squares indicate field measurements of fault attitudes, while white circles mark locations of kinematic indicators. The dashed box outlines the area where the structural analysis of bedding attitudes was performed (panel 3e). Dotted lines represent the axial trace of folds. **(b)** Lower-hemisphere, equal-area projection of fault planes (great circles) measured in the field. Red dots represent kinematic data recorded from striae and/or mineral fibers on fault surfaces within the studied succession. **(c)** Rose diagram, showing strike frequency of faults identified by means of satellite imagery interpretation. **(d)** Rose diagram showing strike frequency of faults surveyed in the field. **(e)** Lower-hemisphere, equal-area projection of bedding poles within the dashed area in panel 3a. The plot includes a best-fit great circle approximating the distribution of bedding poles, concentration contour lines, and the associated π statistical fold axis. Stereographic projections and rose diagrams were created using the Stereonet v.11 software (Richard W. Allmendinger). nf = number of fault data used; nk = number of kinematic indicators; nb = number of bedding attitudes.

to record a minor phase of mild shortening intercalated within the extensional tectonic regime that was dominant throughout the Neogene evolution of the East Pisco Basin. The timing of the deformation unraveled by this study refines previous basin analysis interpretations that overlooked the occurrence of such punctuated shortening events during basin evolution (e.g. Di Celma et al., 2022).

5. Vertebrate paleontology of the study area

Fossil vertebrate remains from the study area have been categorized into either bony or dental elements (see the Main Map). Ninety-one marine vertebrate specimens preserved as bony elements were recorded from the Pisco strata exposed at the study site (Figure 4a). Cetaceans dominate this assemblage, being represented by 76 specimens (corresponding to about 83.5% of the total number) (Figure 4b). Of all the cetacean specimens identifiable at the suborder level, 53 are represented by complete to strongly incomplete skeletons, 34 (37.3%) belong to Mysticeti (baleen-bearing whales) and 21 (20.9%) to Odontoceti (echolocating toothed whales).

Among mysticetes, 13 specimens (14.3%) are identified as members of the extinct family Cetotheriidae, including an exquisitely preserved juvenile skull (Figure 5). Most of these large cetotheriids appear to be referred to an as-yet undescribed, large-bodied, *Piscobalaena*-like taxon whose skeletons are commonly encountered throughout the P1 sequence, e.g. at

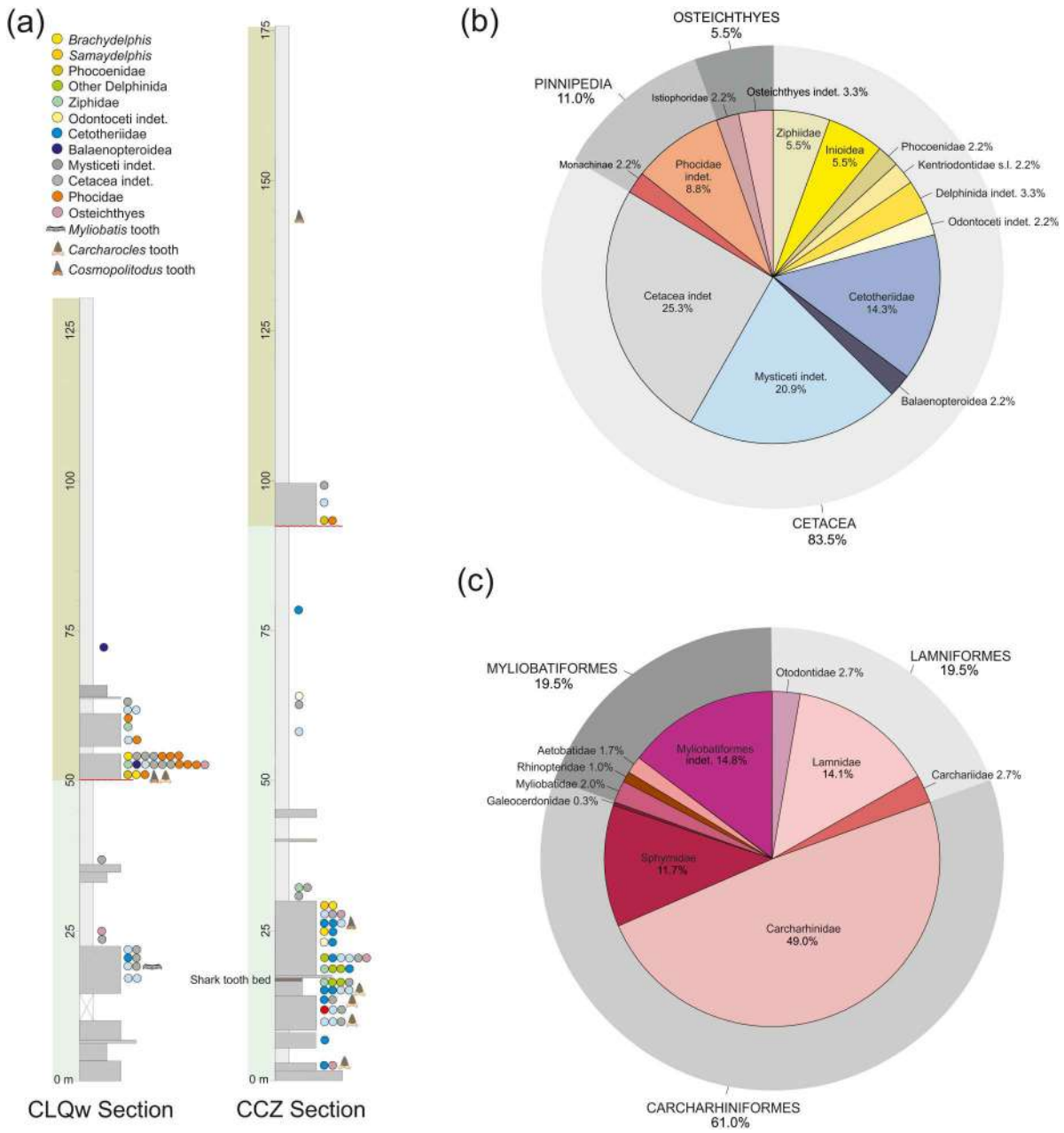

Figure 4. Stratigraphic distribution and taxonomic composition of the fossil vertebrate assemblage from Cerros Cadena de los Zanjones. **(a)** Stratigraphic distribution of marine vertebrate fossil specimens for which precise GPS coordinates are known along the two simplified sedimentary sections (CCZ and CLQw). The green bands represent P1 and P2 sequences; the red line corresponds to the sequence boundary; the horizontal axis represent the grain size distribution. **(b)** Taxonomic composition of the fossil marine vertebrate assemblage from the P1 and P2 strata, based on the systematic surface prospecting of 91 specimens preserved as bony elements. **(c)** Taxonomic composition of the fossil elasmobranch assemblage from the P1 and P2 strata, based on systematic surface prospecting and collection of some 300 dental elements.

Figure 5. Field photographs of mysticete specimens from the study area. **(a)** Excavation of a cranium and mandibles of a juvenile of Cetotheriidae indet. (CCZ52). **(b)** Articulated cranium and mandibles of Cetotheriidae indet. (CCZ13) preserved dorsal side-up.

Cerro Colorado (Bianucci et al., 2016b; Bianucci & Collareta, 2022). Two large mysticete specimens (2.2%) belong to the superfamily Balaenopteroidea, all the remaining records being identified as Mysticeti indet.

Though relatively uncommon, the odontocetes are seemingly more diverse, being represented by different members of Delphinida (the largest toothed whale clade, including many forms of dolphins, porpoises and kin, accounting for 14 specimens, or 13.2%) as well as of Ziphiidae (beaked whales, numbering five, or 5.5%). Specifically, delphinidans include (i) the pontoporiid *Brachydelphis mazeasi* (Figure 6c), a relative of the present-day franciscana (*Pontoporia blainvillei*), and the putative pontoporiid *Samaydelphis chacaltanae* (Figure 6a,b), both of which belong in the superfamily Inioidea (totaling five specimens, or 6.5%) (Figure 4b); (ii) an as-yet undescribed kentriodontid-like basal delphinidan (two specimens, or 2.2%); and (iii) at least two porpoise-like taxa (two specimens, or 2.2%), including an unambiguous member of Phocoenidae. Ziphiids are represented by fragmentary remains (Figure 6d) comprising a total of five specimens (5.5%), including one that may represent *Messapicetus* and two that have previously been assigned to Ziphiidae genus and sp. indet. 1 (Bianucci et al., 2016a, 2024).

Besides cetaceans, the marine vertebrate assemblage is also rich in seals (Pinnipedia, Phocidae) and bony fishes (Osteichthyes). The former group comprises ten specimens (11.0%) and include two skeletons (2.2%) referred to the monk seal subfamily

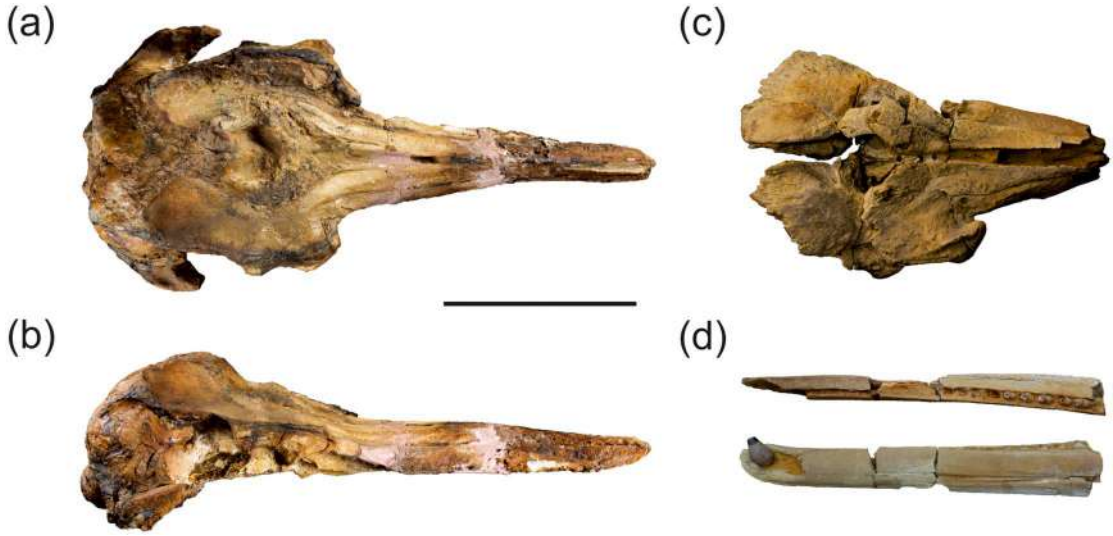

Figure 6. Photographs of odontocete specimens from the study area. **(a,b)** Cranium of *Samaydelphis chacaltanae* (MUSM 3903 = CCZ60) in (a) dorsal and (b) lateral views. **(c)** Fragmentary cranium in dorsal view of *Brachydelphis mazeasi* (CCZ25). **(d)** Symphyseal fragment of left mandible and associated apical tooth of Ziphiidae genus and sp. indet. 1 in dorsal (top) and lateral (bottom) views (MUSM 4966 = CLQC37). Scale bar equals 10 cm.

Monachinae, whereas the latter accounts for five specimens (5.5%) and includes two istiophorid billfishes (2.2%) (Figure 4b).

Most of the aforementioned specimens (63.7%) come from P1 (Figure 4a). Finds are much more common in the sandy lower portions of both sequences (75.8%) rather than in the diatomaceous portions thereof. Just a few skeletons exhibit a high degree of completeness and articulation (Figure 7a), whereas most other specimens for which exhaustive taphonomic data are available are poorly articulated and incomplete, belonging to classes 0–1 of Bosio et al. (2021). The latter also include isolated crania, mandibles, and limb bones, evoking the trend of progressive dismembering of carcasses during flotation as explained by Bosio et al. (2021). Twenty-three cetacean specimens, some four-fifths of which are mysticetes, are found embedded into more or less developed dolomite nodules (Figure 7b–d), which commonly form around large, articulated skeletons after the rapid burial of the carcass (Bosio et al., 2021). Ventrally-disposed skeletons appear to be much more common than the dorsally-disposed ones (Figure 7), with a ratio of about 4:1 based on the available data, which evokes the reflotation of the carcasses after death (Bosio et al., 2021). As few as two specimens were found with associated shark teeth, and just one features shark tooth marks (Figure 7e). Seven specimens were found with associated mollusks, primarily the bivalve *Dosinia* and the gastropod *Turritella* (Figure 7d), which are possibly derived from the shell beds in which the cetacean carcasses sank on.

Elasmobranchs (shark and rays) are represented by some 300 teeth that mostly come from a single diatomite horizon running through P1 some 17 m above the base of the CCZ section (Figure 4a, Figure 8). Among these, there are representatives of Carcharhiniformes (requiem sharks, including Carcharhinidae, Sphyrnidae and Galeocerdonidae, accounting for 61.0% of the teeth), Lamniformes (mackerel sharks, including Lamnidae, Carcharhiidae and Otodontidae, accounting for 19.5% of the teeth) and Myliobatiformes (eagle and cownose rays, including Myliobatidae, Rhinopteridae and Aetobatidae, accounting for 19.5% of the teeth) (Figure 4c). The extant copper shark, *Carcharhinus brachyurus*, is by far the most common elasmobranch species.

The marine mammal assemblage recorded at the study site mostly resembles that from the well-investigated locality of Cerro Colorado, ca. 30 km further northwest, where P1 and P2 are also exposed (Bianucci et al., 2016b; Bosio et al., 2021; Collareta et al., 2021b). Similarities between the two fossil faunas include the shared presence of (i) an as-yet undescribed cetotheriid species for which paleoecological inferences were drawn by Collareta et al. (2015); (ii) the inioid delphinidans *B. mazeasi* and *S. chacaltanae* (Lambert et al., 2021); and, possibly, (iii) the beaked whale *Messapicetus* (Bianucci et al., 2010). All these forms but *B. mazeasi* are limited to P1. Faunal similarities between the study site and Cerro Colorado also include the abundance of teeth referred to *C. brachyurus* from the P1 strata (Landini et al., 2017a, 2017b). The high concentration of vertebrate finds observed within the lowermost 30 m of the CCZ section (Main Map) may correspond to a similar accumulation of fossils observed in the P1 strata at Cerro Colorado (Bianucci et al., 2016b; their Figure 4).

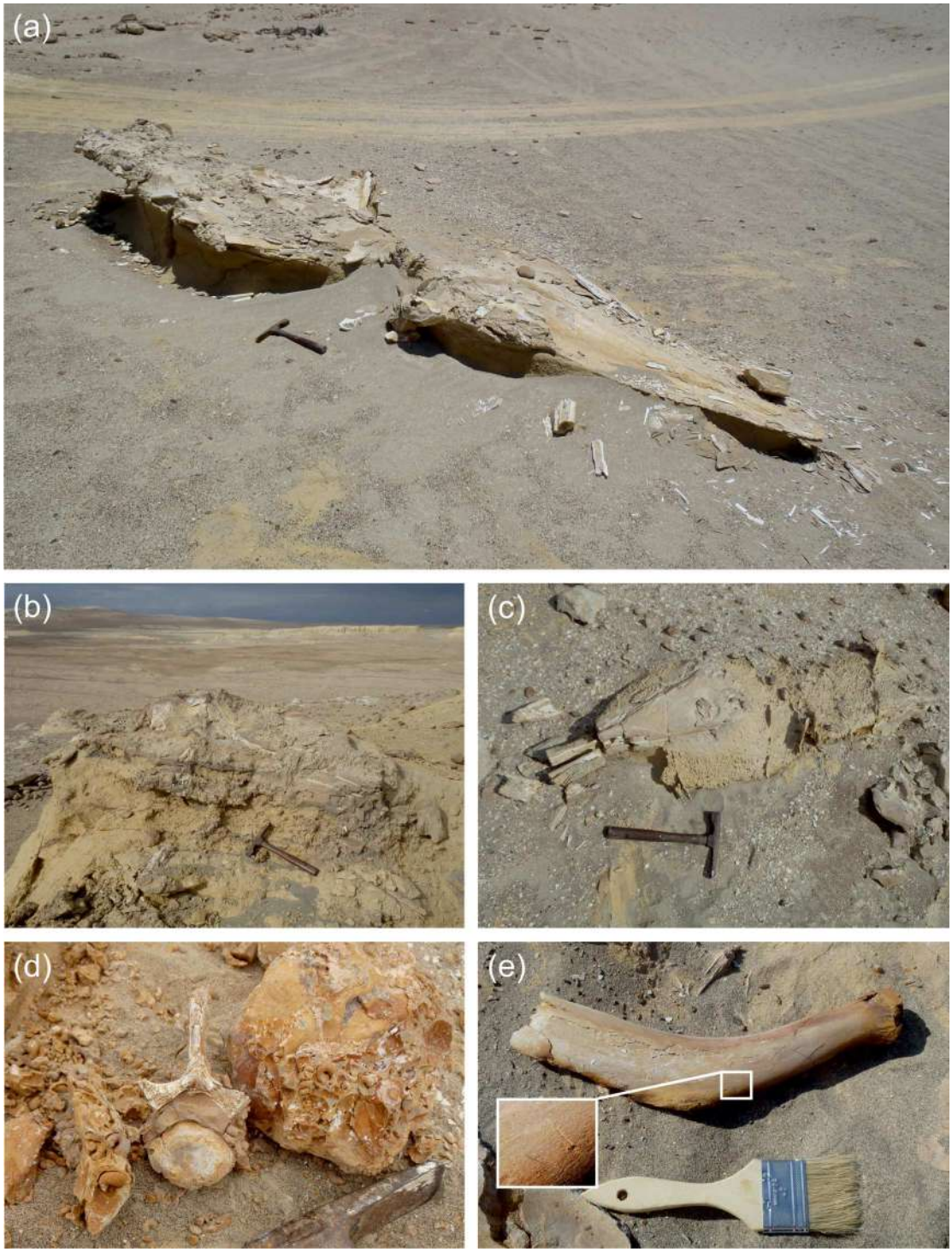

Figure 7. Field photographs exhibiting the main taphonomic features of the fossil marine vertebrates. **(a)** Complete and almost fully articulated skeleton of Cetotheriidae indet. including cranium, articulated mandibles, vertebral column (the thoracics are partially disarticulated) and left scapula, preserved in ventral disposition within a partially developed dolomite nodule (CCZ10). **(b)** Partially eroded cranium of Cetotheriidae indet., preserved in dorsal disposition within a nodule; the postcrania may have been destroyed by erosion (CCZ23). **(c)** Skull, mandible, teeth, and ear bones of Kentriodontidae s.l. n. sp. preserved in ventral disposition and within a nodule (CCZ3). **(d)** Vertebra of Phocidae indet. within a partial nodule with associated internal molds of *Turritella* and other gastropods (CLQC25). **(e)** Rib of Mysticeti indet. displaying shark tooth marks (CLQC11).

At the study site, the P1-P2 passage is marked by the sudden appearance of seals and porpoises (Phocoenidae). This renewed fauna corresponds to the 'CLB vertebrate level' recognized by de Muizon and DeVries (1985) at the locality of Cerro La Bruja, ca. 10 km further northeast (Dewaele & de Muizon, 2024). A faunal turnover is also indicated by the disappearance of the large-bodied cetotheriid species that is very common in the P1 strata, whereas the pontoporiid *Brachydelphis* is found on both sides of the PE0.2 unconformity, as observed in other localities of the East Pisco Basin (Bianucci & Collareta, 2022; Lambert

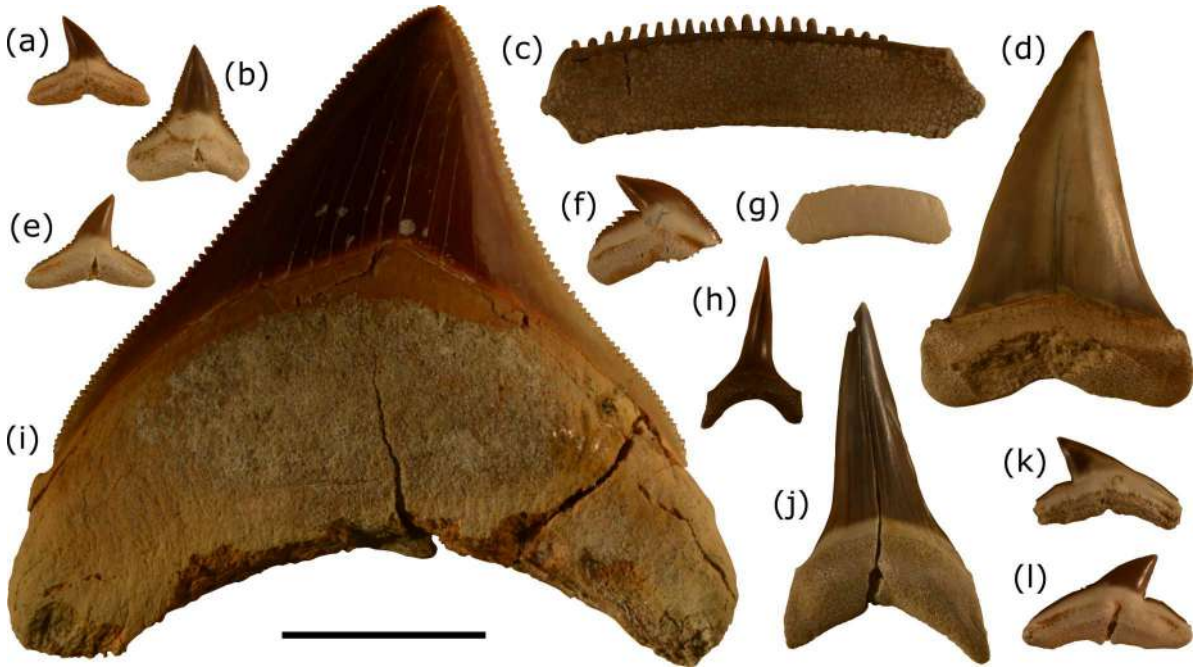

Figure 8. Teeth of Elasmobranchii (sharks and rays) from Cerro Cadena de los Zanjones. **(a,e)** *Carcharhinus brachyurus*; **(b)** *Carcharhinus* cf. *leucas*; **(c,g)** *Myliobatis* sp. (the largest specimen corresponds to CLQC28); **(d,j)** *Cosmopolitodus hastalis*; **(f)** *Galeocerdo aduncus*; **(h)** *Carcharias* sp.; **(i)** *Carcharocles megalodon* (specimen CCZ20); **(k,l)** *Sphyrna* sp. Specimens in panels (c) and (g) are shown in occlusal view; all other specimens are shown in lingual view. Scale bar equals 2 cm.

& de Muizon, 2013). Based on their relatively low stratigraphic position at the base of P2, the phocoenid fossils from the study site (among which is a well-diagnostic periotic) may be the oldest of the whole basin.

6. Concluding remarks

This study provides a comprehensive overview of the Miocene marine vertebrate paleontology and stratigraphy at the locality of Cerros Cadena de los Zanjones, in the Ica River Valley, East Pisco Basin, Peru. In this work, we present a 1:10,000-scale geological map that reports the spatial and temporal distribution of fossil marine vertebrates in the nearby of Cerros Cadena de los Zanjones. Here, the Upper Miocene strata of the Pisco Formation are exposed, including the Tortonian P1 sequence and the Tortonian – Messinian P2 sequence. New and previously published tephrochronological and biostratigraphic dating enabled precise age constraints, shedding light on the temporal span of the fossil assemblage. The Pisco strata exposed in the study area are dated between 9.5–8.6 Ma (P1 sequence) and between 8.4–6.9 Ma (P2). Fossil vertebrates are mostly found in the sandy lower portions of both sequences. They consist of cetaceans, pinnipeds, and bony and cartilaginous fishes. The preservation of the cetacean skeletons, which are often poorly articulated and disposed belly-up, strongly suggests a post-mortem phase of reflotation for most carcasses. The taxonomic composition of the vertebrate assemblage resembles that from the celebrated, nearby locality of Cerro Colorado. A remarkable feature of this assemblage is the abrupt appearance of seals and porpoises and the disappearance of a large-bodied cetotheriid at the P1-P2 boundary. This fossil assemblage conforms to that of the 'CLB vertebrate level' reported by previous workers from Cerro La Bruja, providing further evidence of significant faunal novelties during the Late Miocene. In summary, the data presented herein expand our understanding of the Miocene marine ecosystem of the East Pisco Basin, thus offering new insights into the biodiversity and preservation patterns of marine vertebrates along the southeastern Pacific coasts. Furthermore, this work provides a valuable database for future research while contributing to the valorization and conservation of the exceptional paleontological heritage of the Ica Desert.

Software

The geological map was compiled by scanning hand drafts as black and white TIF files, and then digitizing the line art using the Corel Draw X3 graphics package. The topographic base used for the Main Map was created using the GIS Data processing application Global Mapper 12 to generate contour lines for the 1:10,000 scale topographic base map. The process relied on a digital elevation model (DEM) derived from the Shuttle Radar Topography Mission 26 (SRTM), specifically the SRTM3 dataset provided by the United States Geological Survey (USGS version 2.1). Field data collection was carried out using FieldMOVE (Petroleum

Experts Limited), a digital mapping application designed for geological fieldwork. This tool enables the accurate geolocation of observations and sample positions as well as the measurement of small-scale features directly on digital maps, thus facilitating the efficient gathering and documentation of extensive datasets while enabling real-time visualization of data during fieldwork.

Acknowledgments

Our gratitude goes to Stefania Malagù, Anna Gioncada, Klaas Post, Christian de Muizon, Felix G. Marx, Marco Merella, Karen Gariboldi, Chiara Tinelli, Thomas J. DeVries, Rodolfo Salas-Gismondi, César Chacaltana, Niels Valencia, Walter Aguirre, Ali Altamirano-Sierra, Manuel Laime-Molina, Eusebio Diaz and Joan Chauca-Luyo, for their support in the field and in the lab as well as for many fruitful discussions on the geology and paleontology of the Pisco strata. We are also grateful to Mike Shand, Jose Cuitiño, Alfredo Zurita, the Associate Editor Jasper Knight and the Editor-in-Chief Mike J. Smith for fruitful and helpful comments and suggestions on this work.

Disclosure statement

No potential conflict of interest was reported by the author(s).

Funding

We acknowledge financial support by the European Union – NextGenerationEU, Mission 4, Component 2 CUP I53D23002070 006. Project Title: BIOVERTICES (BIOdiversity of VERTebrates In the CEnozoic Sea). This project is also supported by the Università di Pisa under the ProArcheo 2024 Call for co-funding of Archaeological and Geo-paleontological Research.

Data availability statement

The data that support the findings of this study are available from the authors upon reasonable request.

ORCID

Giulia Bosio http://orcid.org/0000-0001-8067-4926
Alberto Collareta http://orcid.org/0000-0002-6513-8882
Matteo Pedini http://orcid.org/0000-0003-2666-2021
Maria Elena Gastaldello http://orcid.org/0000-0003-1908-9968
Francesco Nobile http://orcid.org/0009-0003-0055-1857
Luca Pellegrino http://orcid.org/0000-0003-2762-9821
Pietro Paolo Pierantoni http://orcid.org/0000-0002-1237-4689
Elisa Malinverno http://orcid.org/0000-0002-9124-5155
Olivier Lambert http://orcid.org/0000-0003-0740-5791
Giuseppe Marramà http://orcid.org/0000-0002-7856-5605
Walter Landini http://orcid.org/0000-0001-7196-9888
Giorgio Carnevale http://orcid.org/0000-0002-3433-4127
Rafael Varas-Malca http://orcid.org/0000-0002-4435-8229
Claudio Di Celma http://orcid.org/0000-0001-7781-7981
Stefano Mazzoli http://orcid.org/0000-0003-3911-9183
Mario Urbina http://orcid.org/0000-0002-1898-9051
Giovanni Bianucci http://orcid.org/0000-0001-7105-0863

References

Allmendinger, R. W., Cardozo, N., & Fisher, D. (2012). *Structural geology algorithms: Vectors and tensors in structural geology* (p. 302). Cambridge University Press.

Bianucci, G., Benites-Palomino, A. M., Collareta, A., Bosio, G., de Muizon, C., Merella, M., Di Celma, C., Malinverno, E., Mario Urbina, M., & Lambert, O. (2024). A new Late Miocene beaked whale (Cetacea, Odontoceti) from the Pisco Formation, and a revised age for the fossil Ziphiidae of Peru. *Bollettino della Società Paleontologica Italiana*, *63*, 21–43. https://doi.org/10.4435/BSPI.2024.10

Bianucci, G., & Collareta, A. (2022). An overview of the fossil record of cetaceans from the East Pisco Basin (Peru). *Bollettino della Società Paleontologica Italiana*, *61*(1), 19–20.

Bianucci, G., Di Celma, C., Collareta, A., Landini, W., Post, K., Tinelli, C., de Muizon, C., Bosio, G., Gariboldi, K., Gioncada, A., Malinverno, E., Cantalamessa, G., Altamirano-Sierra, A., Salas-Gismondi, R., Urbina, M., & Lambert, O. (2016a). Fossil marine vertebrates of Cerro Los Quesos: Distribution of cetaceans, seals, crocodiles, seabirds, sharks, and bony fish in a late Miocene locality of the Pisco Basin, Peru. *Journal of Maps*, *12*(5), 1037–1046. https://doi.org/10.1080/17445647.2015.1115785

Bianucci, G., Di Celma, C., Landini, W., Post, K., Tinelli, C., de Muizon, C., Gariboldi, K., Malinverno, E., Cantalamessa, G., Gioncada, A., Collareta, A., Salas-Gismondi, R., Varas, R., Stucchi, M., Urbina, M., & Lambert, O. (2016b). Distribution of fossil marine vertebrates in Cerro Colorado, the type locality of the giant raptorial sperm whale *Livyatan melvillei* (Miocene, Pisco Formation, Peru). *Journal of Maps*, *12*(3), 543–557. https://doi.org/10.1080/17445647.2015.1048315

Bianucci, G., Di Celma, C., Urbina, M., & Lambert, O. (2016c). New beaked whales from the late Miocene of Peru and evidence for convergent evolution in stem and crown Ziphiidae (Cetacea, Odontoceti). *PeerJ*, *4*, e2479. doi:10.7717/peerj.2479

Bianucci, G., Lambert, O., & Post, K. (2010). High concentration of long-snouted beaked whales (genus *Messapicetus*) from the Miocene of Peru. *Palaeontology*, *53*(5), 1077–1098. https://doi.org/10.1111/j.1475-4983.2010.00995.x

Bosio, G., Bianucci, G., Collareta, A., Landini, W., Urbina, M., & Di Celma, C. (2022). Ultrastructure, composition, and $^{87}Sr/^{86}Sr$ dating of shark teeth from lower Miocene sediments of southern Peru. *Journal of South American Earth Science*, *118*, 103909. https://doi.org/10.1016/j.jsames.2022.103909

Bosio, G., Collareta, A., Di Celma, C., Lambert, O., Marx, F. G., de Muizon, C., Gioncada, A., Gariboldi, K., Malinverno, E., Varas Malca, R., Urbina, M., & Bianucci, G. (2021). Taphonomy of marine vertebrates of the Pisco Formation (Miocene, Peru): Insights into the origin of an outstanding Fossil-Lagerstätte. *PLoS One*, *16*(7), e0254395. https://doi.org/10.1371/journal.pone.0254395

Bosio, G., Gioncada, A., Di Celma, C., Villa, I. M., Pichavant, M., Urbina, M., & Bianucci, G. (2020c). Two-mica rhyolitic tephra in the East Pisco Basin

(Peru): New age and dispersion constraints for the eruptions of the Eastern Cordillera of Central Andes. *Bulletin of Volcanology*, *82*(6), 1–22. https://doi.org/10.1007/s00445-020-1373-y

Bosio, G., Gioncada, A., Malinverno, E., Coletti, G., Collareta, A., Mariani, L., Cavallo, A., Bianucci, G., Urbina, M., & Di Celma, C. (2024). Unraveling marine phosphogenesis along the Miocene coast of Peru: Origin and sedimentological significance of the Pisco Formation phosphorites. *Marine and Petroleum Geology*, 106941. https://doi.org/10.1016/j.marpetgeo.2024.106941

Bosio, G., Gioncada, A., Malinverno, E., Di Celma, C., Villa, I. M., Cataldi, G., Gariboldi, K., Collareta, A., Urbina, M., & Bianucci, G. (2019). Chemical and petrographic fingerprinting of volcanic ashes as a tool for high-resolution stratigraphy of the upper Miocene Pisco Formation (Peru). *Journal of the Geological Society of London*, *176*(1), 13–28. https://doi.org/10.1144/jgs2018-071

Bosio, G., Malinverno, E., Collareta, A., Di Celma, C., Gioncada, A., Parente, M., Berra, F., Marx, F. G., Vertino, A., Urbina, M., & Bianucci, G. (2020a). Strontium isotope stratigraphy and the thermophilic fossil fauna from the Middle Miocene of the East Pisco Basin (Peru). *Journal of South American Earth Science*, *97*, 102399. https://doi.org/10.1016/j.jsames.2019.102399

Bosio, G., Malinverno, E., Villa, I. M., Di Celma, C., Gariboldi, K., Gioncada, A., Barberini, V., Urbina, M., & Bianucci, G. (2020b). Tephrochronology and chronostratigraphy of the Miocene Chilcatay and Pisco formations (East Pisco Basin, Peru). *Newsletters on Stratigraphy*, *53*(2), 213–247. https://doi.org/10.1127/nos/2019/0525

Cardozo, N., & Allmendinger, R. W. (2013). Spherical projections with OSXStereonet. *Computers & Geosciences*, *51*, 193–205. https://doi.org/10.1016/j.cageo.2012.07.021

Chiocci, F. L., & Clifton, H. E. (1991). Gravel-filled gutter casts in nearshore facies – indicators of ancient shoreline trend. In R. H. Osborne (Ed.), *From shoreline to abyss: Contributions in marine geology in honor of Francis Parker Shepard* (Vol. 46, pp. 67–76). SEPM Special Publications.

Ciattoni, S., Cella, F., Mazzoli, S., Zambrano, M., Megna, A., Santini, S., Butler, R., Pierantoni, P. P., & Di Celma, C. (2025). Lithosphere architecture along the axis of the subducting aseismic Nazca Ridge (Peruvian active margin). *Tectonics*, *44*(1), e2024TC008514. https://doi.org/10.1029/2024TC008514

Clift, P. D., & Vannucchi, P. (2004). Controls on tectonic accretion versus erosion in subduction zones: Implications for the origin and recycling of the continental crust. *Review of Geophysics*, *42*(2), 2003RG000127. https://doi.org/10.1029/2003RG000127

Collareta, A., Di Celma, C., Bosio, G., Pierantoni, P. P., Malinverno, E., Lambert, O., Marx, F., Landini, W., Urbina, M., & Bianucci, G. (2021a). Distribution and paleoenvironmental framework of middle Miocene marine vertebrates along the western side of the lower Ica Valley (East Pisco Basin, Peru). *Journal of Maps*, *17*(2), 7–17. https://doi.org/10.1080/17445647.2020.1850535

Collareta, A., Lambert, O., Marx, F. G., de Muizon, C., Varas-Malca, R., Landini, W., Bosio, G., Malinverno, E., Gariboldi, K., Gioncada, A., Urbina, M., & Bianucci, G. (2021b). Vertebrate palaeoecology of the Pisco Formation (Miocene, Peru): Glimpses into the ancient Humboldt Current ecosystem. *Journal of Marine Science and Engineering*, *9*(11), 1188. https://doi.org/10.3390/jmse9111188

Collareta, A., Landini, W., Lambert, O., Post, K., Tinelli, C., Di Celma, C., Panetta, D., Tripodi, M., Salvadori, P. A., Caramella, D., Marchi, D., Urbina, M., & Bianucci, G. (2015). Piscivory in a Miocene Cetotheriidae of Peru: First record of fossilized stomach content for an extinct baleen-bearing whale. *The Science of Nature*, *102*(11-12), 1–12. https://doi.org/10.1007/s00114-015-1319-y

de Muizon, C. (1981). Les vertébrés fossils de la Formation Pisco (Pérou). Première partie: Deux nouveaux Monachinae (Phocidae: Mammalia) du Pliocène de Sud Sacaco. *Travaux de l'Institut Français d'Etudes Andines*, *6*, 20–161.

de Muizon, C. (1988). Les vertébrés de la Formation Pisco (Pérou). Troisième partie: Les Odontocètes (Cetacea, Mammalia) du Miocène. *Travaux de l'Institut Français d'Etudes Andines*, *42*, 1–244.

de Muizon, C., & DeVries, T. J. (1985). Geology and paleontology of late Cenozoic marine deposits in the Sacaco area (Peru). *Geologische Rundschau*, *74*(3), 547–563. doi:10.1007/BF01821211

Dewaele, L., & de Muizon, C. (2024). A new monachine seal (Monachinae, Phocidae, Mammalia) from the Miocene of Cerro La Bruja (Ica department, Peru). *Geodiversitas*, *46*(3), 31–100. https://doi.org/10.5252/geodiversitas2024v46a3

Di Celma, C., Malinverno, E., Bosio, G., Collareta, A., Gariboldi, K., Gioncada, A., Molli, G., Basso, D., Varas-Malca, R., Pierantoni, P. P., Villa, I. M., Lambert, O., Landini, W., Sarti, G., Cantalamessa, G., Urbina, M., & Bianucci, G. (2017). Sequence stratigraphy and paleontology of the upper miocene Pisco Formation along the western side of the lower Ica valley (Ica Desert, Peru). *Rivista. Italiana di Paleontologia e Stratigrafia*, *123*, 255–273. https://doi.org/10.13130/2039-4942/8373

Di Celma, C., Malinverno, E., Bosio, G., Gariboldi, K., Collareta, A., Gioncada, A., Landini, W., Pierantoni, P. P., & Bianucci, G. (2018a). Intraformational unconformities as a record of late Miocene eustatic falls of sea level in the Pisco Formation (southern Peru). *Journal of Maps*, *14*(2), 607–619. https://doi.org/10.1080/17445647.2018.1517701

Di Celma, C., Malinverno, E., Cantalamessa, G., Gioncada, A., Bosio, G., Villa, I. M., Gariboldi, K., Rustichelli, A., Pierantoni, P. P., Landini, W., & Tinelli, C. (2016a). Stratigraphic framework of the late Miocene Pisco Formation at Cerro Los Quesos (Ica Desert. Peru). *Journal of Maps*, *12*(5), 1020–1028. doi:10.1080/17445647.2015.1115783

Di Celma, C., Malinverno, E., Collareta, A., Bosio, G., Gariboldi, K., Lambert, O., Landini, W., Pierantoni, P. P., Gioncada, A., Villa, I. M., Coletti, G., de Muizon, C., Urbina, M., & Bianucci, G. (2018b). Facies analysis, stratigraphy and marine vertebrate assemblage of the lower Miocene Chilcatay Formation at Ullujaya (Pisco Basin, Peru). *Journal of Maps*, *14*(2), 257–268. https://doi.org/10.1080/17445647.2018.1456490

Di Celma, C., Malinverno, E., Gariboldi, K., Gioncada, A., Rustichelli, A., Pierantoni, P. P., Landini, W., Bosio, G., Tinelli, C., & Bianucci, G. (2016b). Stratigraphic framework of the late Miocene to Pliocene Pisco Formation at Cerro Colorado (Ica Desert. Peru). *Journal of Maps*, *12*(3), 515–529. doi:10.1080/17445647.2015.1047906

Di Celma, C., Pierantoni, P. P., Malinverno, E., Collareta, A., Lambert, O., Landini, W., Bosio, G., Gariboldi, K.,

Gioncada, A., de Muizon, C., Molli, G., Marx, F. G., Varas-Malca, R. M., Urbina, M., & Bianucci, G. (2019). Allostratigraphy and paleontology of the lower Miocene Chilcatay Formation in the Zamaca area, East Pisco Basin, southern Peru. *Journal of Maps*, *15*(2), 393–405. https://doi.org/10.1080/17445647.2019.1604439

Di Celma, C., Pierantoni, P. P., Volatili, T., Molli, G., Mazzoli, S., Sarti, G., Ciattoni, S., Bosio, G., Malinverno, E., Collareta, A., Gariboldi, K., Gioncada, A., Jablonska, D., Landini, W., Urbina, M., & Bianucci, G. (2022). Towards deciphering the Cenozoic evolution of the East Pisco basin (southern Peru). *Journal of Maps*, *18*(2), 397–412. https://doi.org/10.1080/17445647.2022.2072780

Fisher, R. V., & Schmincke, H.-U. (1984). *Pyroclastic rocks*. Springer.

Gariboldi, K., Bosio, G., Malinverno, E., Gioncada, A., Di Celma, C., Villa, I. M., Urbina, M., & Bianucci, G. (2017). Biostratigraphy, geochronology and sedimentation rates of the upper Miocene Pisco Formation at two important marine vertebrate fossil-bearing sites of southern Peru. *Newsletters on Stratigraphy*, *50*(4), 417–444. https://doi.org/10.1127/nos/2017/0345

Gariboldi, K., Gioncada, A., Bosio, G., Malinverno, E., Di Celma, C., Tinelli, C., Cantalamessa, G., Landini, W., Urbina, M., & Bianucci, G. (2015). The dolomite nodules enclosing fossil marine vertebrates in the East Pisco Basin, Peru: Field and petrographic insights into the Lagerstätte formation. *Palaeogeography, Palaeoclimatology, Palaeoecology*, *438*, 81–95. doi:10.1016/j.palaeo.2015.07.047

Gariboldi, K., Pike, J., Malinverno, E., Di Celma, C., Gioncada, A., & Bianucci, G. (2023). Paleoceanographic implications of diatom seasonal laminations in the Upper Miocene Pisco Formation (Ica desert, Peru) and their clues on the development of the Pisco Fossil-Lagerstätte. *Paleoceanography and Paleoclimatology*, *38*(5), e2022PA004566. https://doi.org/10.1029/2022PA004566

Gioncada, A., Collareta, A., Gariboldi, K., Lambert, O., Di Celma, C., Bonaccorsi, E., Urbina, M., & Bianucci, G. (2016). Inside baleen: Exceptional microstructure preservation in a late Miocene whale skeleton from Peru. *Geology*, *44*(10), 839–842. https://doi.org/10.1130/G38216.1

Gioncada, A., Gariboldi, K., Collareta, A., Di Celma, C., Bosio, G., Malinverno, E., Lambert, O., Pike, J., Urbina, M., Bianucci, G., & Bianucci, G. (2018). Looking for the key to preservation of fossil marine vertebrates in the Pisco Formation of Peru: New insight from a small dolphin skeleton. *Andean Geology*, *45*(3), 379–398. https://doi.org/10.5027/andgeoV45n3-3122

Herbozo, G., Kukowski, N., Clift, P. D., Pecher, I., & Bolaños, R. (2020). Cenozoic increase in subduction erosion during plate convergence variability along the convergent margin off Trujillo, Peru. *Tectonophysics*, *790*, 228557. https://doi.org/10.1016/j.tecto.2020.228557

Kulm, L. D., Resig, J. M., Thornburg, T. M., & Schrader, H. J. (1982). Cenozoic structure, stratigraphy and tectonics of the central Peru forearc. In J. K. Legget (Ed.), *Trench and forearc geology: Sedimentation and tectonics on modern and ancient plate margins* (pp. 151–169). Blackwell.

Lambert, O., Bianucci, G., Post, K., de Muizon, C., Salas-Gismondi, R., Urbina, M., & Reumer, J. (2010). The giant bite of a new raptorial sperm whale from the Miocene epoch of Peru. *Nature*, *466*(7302), 105–108. https://doi.org/10.1038/nature09067

Lambert, O., Collareta, A., Benites-Palomino, A., Di Celma, C., De Muizon, C., Urbina, M., & Bianucci, G. (2021). A new small, mesorostrine inioid (Cetacea, Odontoceti, Delphinida) from four upper Miocene localities in the Pisco Basin, Peru. *Papers in Palaeontology*, *7*(2), 1043–1064. https://doi.org/10.1002/spp2.1332

Lambert, O., & de Muizon, C. (2013). A new long-snouted species of the Miocene pontoporiid dolphin Brachydelphis and a review of the Mio-Pliocene marine mammal levels in the Sacaco Basin, Peru. *Journal of Vertebrate Paleontology*, *33*(3), 709–721. doi:10.1080/02724634.2013.743405

Landini, W., Altamirano-Sierra, A., Collareta, A., Di Celma, C., Urbina, M., & Bianucci, G. (2017a). The late Miocene elasmobranch assemblage from Cerro Colorado (Pisco Formation, Peru). *Journal of South American Earth Sciences*, *73*, 168–190. https://doi.org/10.1016/j.jsames.2016.12.010

Landini, W., Collareta, A., Pesci, F., Di Celma, C., Urbina, M., & Bianucci, G. (2017b). A secondary nursery area for the copper shark *Carcharhinus brachyurus* from the late Miocene of of Peru. *Journal of South American Earth Sciences*, *78*, 164–174. https://doi.org/10.1016/j.jsames.2017.07.003

Lazarus, D., Barron, J., Renaudie, J., Diver, P., & Türke, A. (2014). Cenozoic planktonic marine diatom diversity and correlation to climate change. *PLoS One*, *9*(1), e84857. https://doi.org/10.1371/journal.pone.0084857

Leckie, D. A., & Walker, R. G. (1982). Storm- and tide-dominated shorelines in Cretaceous Moosebar-Lower Gates interval: Outcrop equivalents of Deep Basin gas trap in western Canada. *American Association of Petroleum Geologists Bulletin*, *66*, 138–157. https://doi.org/10.1306/03B59A53-16D1-11D7-8645000102C1865D

Malinverno, E., Bosio, G., Gastaldello, M. E., Pellegrino, L., Bianucci, G., Collareta, A., Gariboldi, K., Urbina, M., Villa, I. M., & Di Celma, C. (2025). The early depositional history of the Pisco Formation (Miocene, Peru). *Newsletters on Stratigraphy*. https://doi.org/10.1127/nos/2025/0864

Malinverno, E., Bosio, G., Gioncada, A., Cimò, R., Andò, S., Mariani, L., Coletti, G., Boschi, C., Gariboldi, K., Galimberti, L., Bianucci, G., Urbina, M., & Di Celma, C. (2023). Laterally continuous dolomite layers of the Miocene Pisco Formation (East Pisco Basin, Peru): A window into past cyclical changes of the diagenetic environment. *Marine and Petroleum Geology*, *147*, 105977. https://doi.org/10.1016/j.marpetgeo.2022.105977

Myrow, P. M. (1992). Pot and gutter casts from the Chapel Island Formation, southeast Newfoundland. *Journal of Sedimentary Petrology*, *62*(6), 992–1007. https://doi.org/10.2110/jsr.62.992

Noda, A. (2016). Forearc basins: Types, geometries, and relationships to subduction zone dynamics. *Geological Society of America Bulletin*, *128*(1), 879–895. doi:10.1130/B31345.1

Patacci, M. (2016). A high-precision Jacob's staff with improved spatial accuracy and laser sighting capability. *Sedimentary Geology*, *335*, 66–69. https://doi.org/10.1016/j.sedgeo.2016.02.001

Romero, D., Valencia, K., Alarcón, P., Peña, D., & Ramos, V. A. (2013). The offshore basement of Peru: Evidence for different igneous and metamorphic domains in the forearc. *Journal of South American Earth Sciences*, *42*, 47–60. https://doi.org/10.1016/j.jsames.2012.11.003

Stucchi, M., Varas-Malca, R. M., & Urbina-Schmitt, M. (2015). New Miocene sulid birds from Peru and considerations on their Neogene fossil record in the Eastern Pacific Ocean. *Acta Palaeontologica Polonica*, *61*(2), 417–427.

Tewksbury, B. J., Dokmak, A. A. K., Tarabees, E. A., & Mansour, A. S. (2012). Google Earth and geologic research in remote regions of the developing world; an example from the Western Desert of Egypt. In S. J. Whitmeyer, J. E. Bailey, D. G. De Paor, & T. Ornduff (Eds.), *Google earth and virtual visualizations in geoscience education and research* (Vol. 492, pp. 23–36). Geological Society of America Special Paper.

Thornburg, T. M., & Kulm, L. D. (1981). Sedimentary basins of the Peru continental margin: Structure, stratigraphy, and Cenozoic tectonics from 6∘S to 16∘S latitude. In L. D. Kulm, J. Dymond, E. J. Dasch, & D. M. Hussong (Eds.), *Nazca plate: Crustal formation and andean convergence* (Vol. 154, pp. 393–422). Geological Society of America, Memoir.

Travis, R. B., Gonzales, G., & Pardo, A. (1976). Hydrocarbon potential of coastal basins of Peru. *AAPG Memoir*, *25*, 331–338. https://doi.org/10.1306/83D918CB–16C7–11D7–8645000102C1865D

Viveen, W., & Schlunegger, F. (2018). Prolonged extension and subsidence of the Peruvian forearc during the Cenozoic. *Tectonophysics*, *730*, 48–62. https://doi.org/10.1016/j.tecto.2018.02.018

von Huene, R., & Suess, E. (1988). Ocean drilling program Leg 112, Peru continental margin. *Geology*, *16*(10), 934–938. https://doi.org/10.1130/0091-7613(1988)016<0934:ODPLPC>2.3.CO;2

Miocene stratigraphy and vertebrate paleontology along the western side of Cerros Cadena de los Zanjones (Ica Desert, Peru)

Bosio G.[(1)], Collareta A.[(1)], Pedini M.[(2)], Gastaldello M.E.[(3)], Nobile F.[(1)], Pellegrino L.[(4)], Pierantoni P.P.[(2)], Malinverno E.[(3)], Lambert O.[(5)], Marramà G.[(4)], Landini W.[(1)], Carnevale G.[(4)], Varas-Malca R.[(6, 7)], Di Celma C.[(2)], Mazzoli S.[(2)], Urbina M.[(6)], Bianucci G.[(1)]

(1) Dipartimento di Scienze della Terra, Università di Pisa, Pisa, Italy
(2) Scuola di Scienze e Tecnologie, Università di Camerino, Camerino, Italy
(3) Dipartimento di Scienze dell'Ambiente e della Terra, Università di Milano-Bicocca, Milan, Italy
(4) Dipartimento di Scienze dell'Ambiente e della Terra, Università di Torino, Turin, Italy
(5) D.O. Terre et Histoire de la Vie, Institut Royal des Sciences Naturelles de Belgique, Brussels, Belgium
(6) Departamento de Paleontología de Vertebrados, Museo de Historia Natural-UNMSM, Lima, Peru
(7) Unidad de Paleontología, Museo de Historia Natural, Universidad Ricardo Palma, Lima, Peru

Project funded by the European Union–Next Generation EU, Mission 4, Component 2 CUP I53D23002070 006.
Project title: "BIOdiversity of VERTebrates In the CEnozoic Sea" (BIO- VERTICES)

STUDY AREA

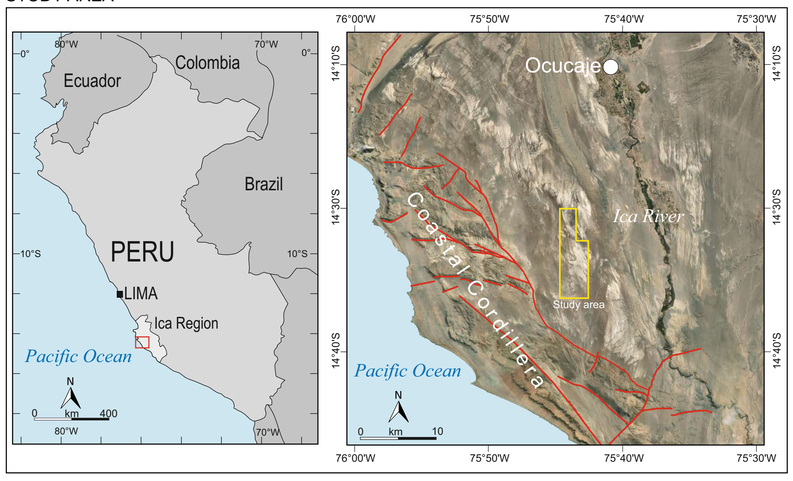

PISCO BASIN CHRONOSTRATIGRAPHIC CHART

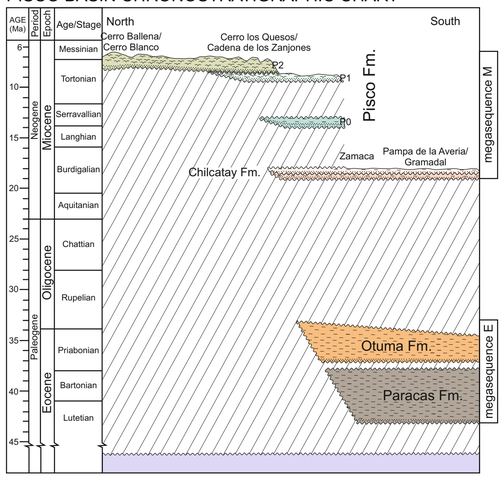

LEGEND

Quaternary surficial map units

Eolian sands

Pisco Formation (Upper Miocene)

In the study area, it comprises two high-frequency sequences of shelfal origin, namely, P1 and P2. The vertical progression of sedimentary facies associations within each sequence displays an overall fining-upward trend that includes nearshore conglomerates and thoroughly bioturbated, fine-grained sandstones transitioning upwards into offshore diatomaceous mudstones with minor additions of sandstones, dolomitic horizons, and ash layers.

Árbol
Araña
Alcatraz
P2 High-order sequence
PE0.2 unconformity
P1 High-order sequence

Symbols

4° Strike and dip of bedding
Normal faults (rectangles on downthrown block)
Undistinct normal faults
Anticline (a) and syncline (b) axial trace

Fossils

Odontoceti
Mysticeti
Cetacea indet.
Phocidae
Osteichthyes
Myliobatis tooth
Carcharocles tooth
Cosmopolitodus tooth

Biostatigraphic events and radiometric dating

First Occurrence (FO) or Last Occurrence (LO) data of selected taxa, correlated with global FAD or LAD
First Occurrence or Last Occurrence of selected taxa, interpreted as representing local conditions
$^{40}Ar/^{39}Ar$ radiometric dating

Lithological sections

Volcanic ash
Laminated diatomites
Nodules
Basement clasts
Mollusk shells
Gyrolithes
Phosphorite nodules and mollusk shells

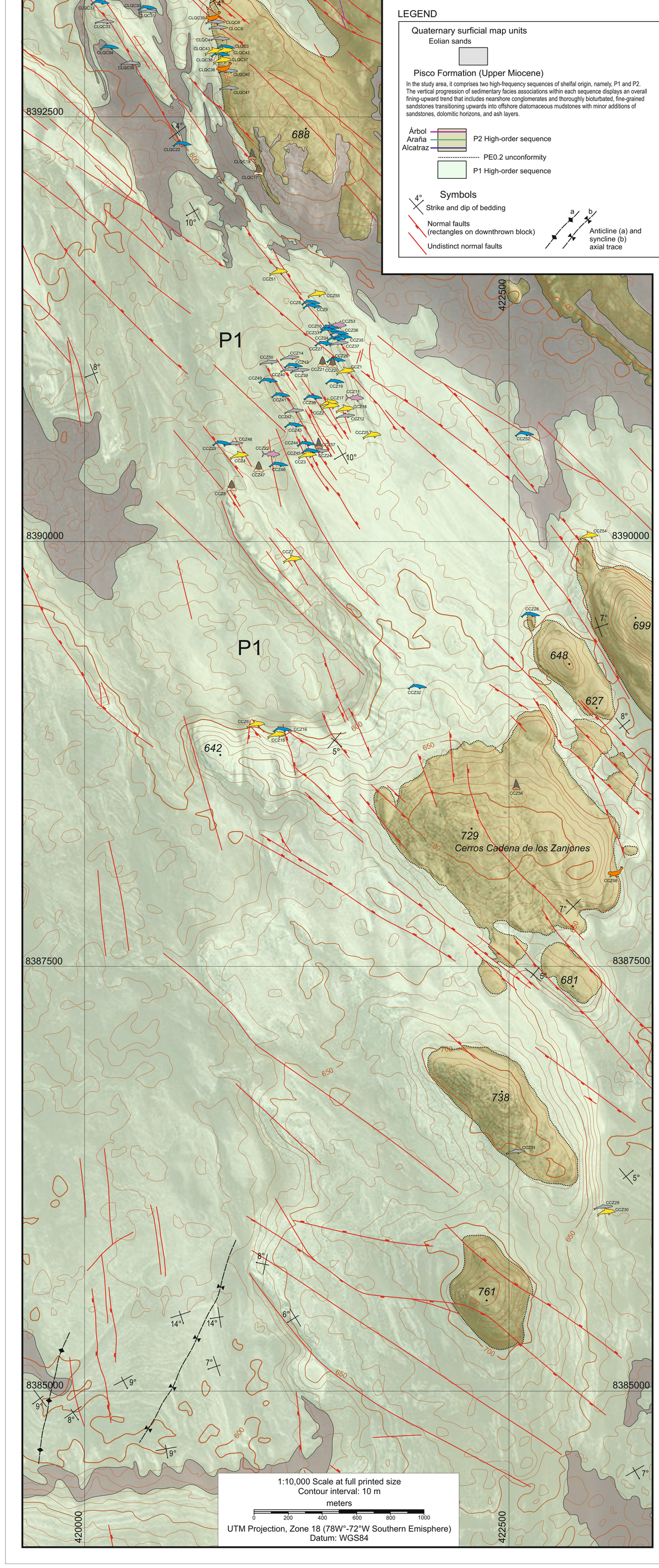

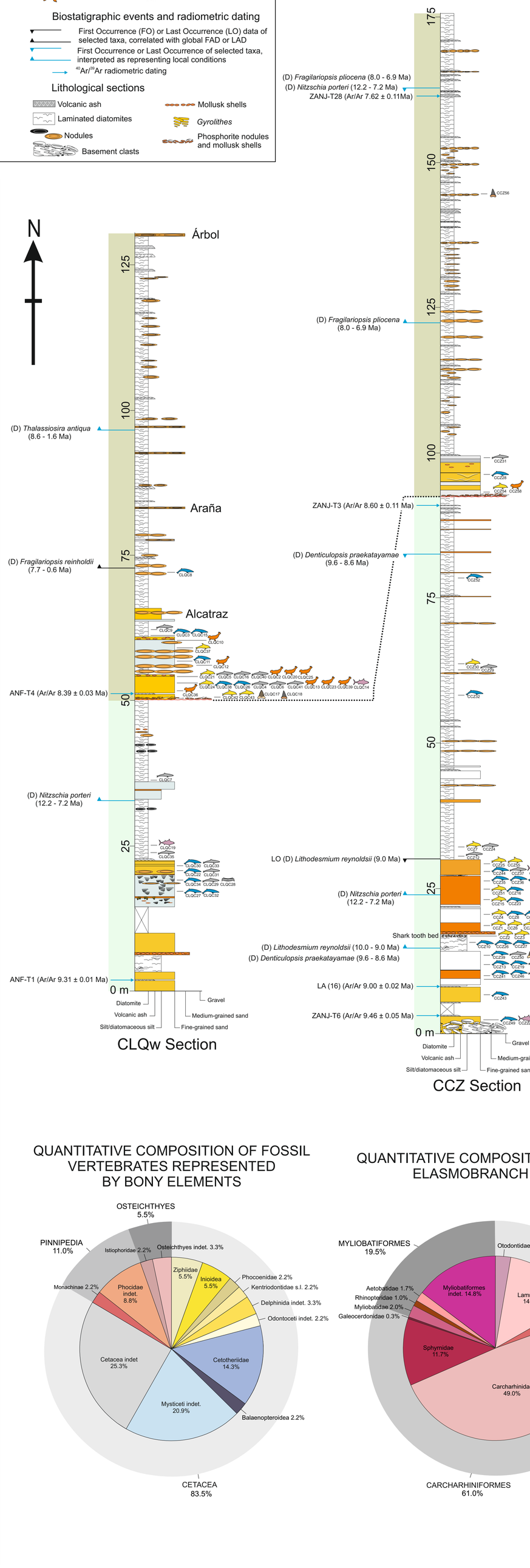

HEIGHT IN THE STRATIGRAPHIC SUCCESSION AND PRELIMINARY SYSTEMATIC DETERMINATION OF FOSSIL VERTEBRATES

Odontoceti | Mysticeti | Cetacea indet. | Phocidae | Osteichthyes | Elasmobranchi

Cerro los Quesos West

Field number	Height abs (m)	Determination	Description
CLQC2	54.0	Phocidae indet.	Eroded femur
CLQC3	61.2	Mysticeti indet.	Mandible fragments and large lumbars and caudals of balaenopteroid-sized mysticete
CLQC4	53.3	Cetacea indet.	Vertebrae of medium-sized cetacean
CLQC5	54.0	Cetacea indet.	Posterior caudal vertebrae of large-sized balaenopteroid-like cetacean
CLQC6	53.3	Cetacea indet.	Ulna, phalanges and bone fragments of cetotheriid-sized cetacean
CLQC7	36.4	Cetacea indet.	Articulated vertebral column of cetotheriid-sized cetacean
CLQC8	72.0	Balaenopteridea indet.	Large fragmentary cranium and vertebrae
CLQC9	62.2	Cetacea indet.	Vertebrae and ribs of cetotheriid-sized cetacean
CLQC10	60.4	Monachinae indet.	Eroded skull, vertebrae, ribs, scapula, humerus and phalanges
CLQC11	56.8	Mysticeti indet.	Large partial cranium and rib with small shark tooth mark
CLQC12	56.1	Phocidae indet.	Eroded and partially dislocated skeleton including articulated vertebrae, fragments of limb bones (femur) and ribs
CLQC13	52.8	Phocidae indet.	Scapula
CLQC14	53.3	Osteichthyes indet.	Bone fragments
CLQC15	61.2	Mysticeti indet.	Eroded mandible
CLQC16	50.5	Cetacea indet.	Articulated thoracic vertebrae and ribs of small cetacean
CLQC17	50.7	*Carcharocles megalodon*	Fragmentary tooth
CLQC18	50.7	*Cosmopolitodus* sp.	Tooth
CLQC19	25.2	Istiophoridae indet.	Skull
CLQC20	54.0	Monachinae indet.	Cranium (MUSM 2531)
CLQC21	54.0	*Brachydelphis mazeasi*	Eroded cranium
CLQC22	20.9	Cetotheriidae indet.	Cranium
CLQC23	52.8	Phocidae indet.	Scapula
CLQC24	52.8	Ziphiidae gen. et sp. indet. 1	Eroded, partially destroyed skeleton. Fragments of skull, mandibles and ear bones (MUSM 3237)
CLQC25	54.0	Phocidae indet.	Vertebrae and eroded bone fragments
CLQC26	52.8	Mysticeti indet.	Cranium and mandibles with disarticulated scapula and ribs
CLQC27	17.6	Mysticeti indet.	Dislocated portions of cetotheriid-sized skeleton, including articulated cervicals, thoracics and ribs
CLQC28	18.7	*Myliobatis* sp.	Tooth
CLQC29	18.7	Cetacea indet.	Dislocated large vertebra
CLQC30	21.7	Mysticeti indet.	Destroyed cranium
CLQC31	20.9	Cetacea indet.	Destroyed large cranium
CLQC32	17.6	Mysticeti indet.	Dislocated fragments of cranium, vertebrae and ribs
CLQC33	21.7	Cetacea indet.	Dislocated and destroyed large cranium of mysticete-sized cetacean
CLQC34	19.3	Mysticeti indet.	Partially articulated eroded skeleton, inside a nodule, with fragments of mandibles, vertebrae and ribs exposed
CLQC35	24.0	Cetacea indet.	Two vertebrae (other parts of skeleton may dwell in a nodule)
CLQC36	51.7	Phocidae indet.	Cranium
CLQC37	59.1	Ziphiidae gen. et sp. indet. 1	Eroded and dislocated fragmentary skeleton including cranial bones, mandibles and teeth (MUSM 4966)
CLQC38	53.3	Balaenopteridea indet.	Cranium in ventral view with exposed bullae
CLQC39	53.3	Phocidae indet.	Fragmentary limb bones
CLQC40	54.0	Cetacea indet.	Dislocated vertebrae of small *Brachydelphis*-like cetacean
CLQC41	52.8	Cetacea indet.	Vertebrae and ribs
CLQC42	50.7	*Brachydelphis* sp.	Left periotic
CLQC43	50.7	Phocoenidae indet.	Right periotic

Cerros Cadena de los Zanjones

Field number	Height abs (m)	Determination	Description
CCZ1	19.1	aff. Ziphiidae indet.	Skull, mandibles (with large alveoli) and vertebrae
CCZ2	16.8	Delphinida indet.	Small cranium
CCZ3	16.8	Kentriodontidae s.l. n. sp.	Skull, mandible, teeth, ear bones, large teeth; ear bones similar to CCZ-4
CCZ4	20.4	Kentriodontidae s.l. n. sp.	Skull and mandible fragments with large teeth; ear bones similar to CCZ-3
CCZ5	2.3	*Carcharocles megalodon*	Tooth
CCZ6	18.3	Delphinida indet.	Disarticulated cranium, mandible fragments, ear bones and some vertebrae
CCZ7	32.2	aff. Ziphiidae indet.	Skull, mandibles, vertebrae and forelimb (humerus + ulna); same size of *Messapicetus* and ziphiid-like humerus
CCZ8	20.4	Cetotheriidae indet.	Partially eroded cranium with articulated mandibles and disarticulated vertebrae and ribs
CCZ9	18.3	Cetotheriidae indet.	Eroded skeleton, including dislocated and broken cranium
CCZ10	16.2	Cetotheriidae indet.	Complete and almost fully articulated skeleton, including cranium, mandibles, vertebral column and left scapula
CCZ11	21.1	Osteichthyes indet.	Skull
CCZ12	30.6	Cetacea indet.	4-5 disarticulated cetotheriid-sized caudal vertebrae
CCZ13	11.9	Cetotheriidae indet.	Partially articulated skeleton including cranium, mandibles and vertebrae
CCZ14	11.9	Cetacea indet.	Cetotheriid-sized, disarticulated and eroded vertebrae and bone fragments
CCZ15	22.8	Odontoceti indet.	Partial skeleton, including cranium and mandibles, humerus, ulna, vertebrae and some rib fragments; postcrania partially dislocated
CCZ16	24.5	Cetotheriidae indet.	Cranium and articulated mandibles
CCZ17	18.3	Delphinida indet.	Small tympanic bulla and vertebrae
CCZ18	16.8	aff. *Messapicetus* sp.	Eroded and dislocated neurocranium
CCZ19	11.9	Mysticeti indet.	Disarticulated cranium, mandibles, and vertebrae of cetotheriid-sized mysticete
CCZ20	15.3	*Carcharocles megalodon*	Tooth
CCZ21	9.3	*Carcharocles megalodon*	Tooth fragment
CCZ22	2.3	Osteichthyes indet.	Vertebra
CCZ23	23.3	Cetotheriidae indet.	Partially eroded cranium (postcrania may have been destroyed by erosion)
CCZ24	32.2	Cetacea indet.	6-7 eroded and partially articulated cetotheriid-sized vertebrae
CCZ25	29.6	*Brachydelphis mazeasi*	Destroyed and partially dislocated skeleton including incomplete cranium, vertebrae and ribs
CCZ26	16.2	Cetotheriidae indet.	Eroded cranium and articulated mandibles
CCZ27	16.2	Mysticeti indet.	Eroded cranium
CCZ28	96.3	Mysticeti indet.	Eroded and partially dislocated skeleton of cetotheriid-like mysticete including disarticulated vertebrae and ribs and articulated forelimb (humerus, radius, ulna and metacarpals) and sternal bone
CCZ29	63.3	Cetacea indet.	Thoracic vertebra
CCZ30	63.7	Odontoceti indet.	Partially disarticulated postcrania, including vertebrae, ribs, sternum, articulated radius, ulna and humerus of small *Brachydelphis*-like odontocete
CCZ31	99.2	Cetacea indet.	Bone fragment (rib or mysticete mandible)
CCZ32	58.3	Mysticeti indet.	Eroded and dislocated mandible
CCZ33	15.3	Mysticeti indet.	Skeleton in nodule
CCZ34	20.4	Mysticeti indet.	Destroyed skeleton, including cranium and vertebrae
CCZ35	26.3	Cetotheriidae indet.	Eroded cranium and partial articulated vertebral column
CCZ36	26.3	Cetotheriidae indet.	Cranium, articulated mandible and complete articulated vertebral column
CCZ37	27.9	Cetacea indet.	Large dislocated vertebrae and ribs
CCZ38	20.4	Mysticeti indet.	Destroyed mandible + ?cranium
CCZ39	13.4	Cetacea indet.	Destroyed and dislocated cranium of cetotheriid-sized mysticete
CCZ40	16.8	Cetacea indet.	Destroyed and dislocated vertebrae and ?rostrum
CCZ41	9.3	Mysticeti indet.	Eroded cranium and mandible
CCZ42	9.3	Cetacea indet.	Vertebrae and ribs of cetotheriid-size cetacean fallen from a cliff
CCZ43	6.7	Cetotheriidae indet.	Partially destroyed cranium, mandibles and cervical vertebrae
CCZ44	27.9	Mysticeti indet.	Partially destroyed skeleton, including vertebrae, ribs and dislocated cranium
CCZ45	26.3	Mysticeti indet.	Articulated vertebral column associated with a tooth of *Cosmopolitodus* (CCZ59)
CCZ46	10.0	Mysticeti indet.	Disarticulated partially eroded cranium, mandibles and ribs
CCZ47	13.4	*Carcharocles megalodon*	Tooth fragment
CCZ48	20.4	Cetacea indet.	Partially articulated large vertebrae
CCZ49	2.3	Cetotheriidae indet.	Skeleton partially covered by sand: visible fragmentary cranium, mandibles and vertebrae; eroded and partially disarticulated
CCZ50	14.0	Cetacea indet.	Partially destroyed cranium and vertebrae of mysticete-size cetacean
CCZ51	25.3	*Brachydelphis mazeasi*	Cranium
CCZ52	78.5	Cetotheriidae indet.	Cranium and disarticulated mandibles of juvenile cetotheriid
CCZ53	27.9	Istiophoridae indet.	Skull
CCZ54	93.2	aff. Phocoenidae indet.	Left periotic and vertebral epiphysis
CCZ55	29.6	*Samaydelphis chacaltanae*	Isolated cranium (MUSM 3903)
CCZ56	144.5	*Cosmopolitodus* sp.	Tooth
CCZ57	26.3	*Cosmopolitodus hastalis*	Tooth associated with the CCZ45 mysticete skeleton
CCZ58	93.2	Phocidae indet.	Radius

QUANTITATIVE COMPOSITION OF FOSSIL VERTEBRATES REPRESENTED BY BONY ELEMENTS

QUANTITATIVE COMPOSITION OF FOSSIL ELASMOBRANCH TEETH